

Fig. 1. Plane-strain dual circular tunnels in cohesive-frictional soil.

Fig. 2. Finite element mesh for  $H/D=1$  and  $S/D=2$  showing boundary conditions for numerical limit analysis.

Fig. 3. Upper-bound rigid-block mechanisms for dual circular tunnels.

- (a) mechanism 1
- (b) mechanism 2
- (c) mechanism 3

Fig. 4. Comparison of rigid-block mechanism with finite element limit analysis ( $H/D=1$ ,  $\phi'=10^\circ$ ,  $\gamma D/c'=1$ ,  $S/D=1.5$ , smooth interface).

- (a) Plastic multiplier field
- (b) Power dissipation
- (c) Rigid-block mechanism

Fig. 5. Comparison of rigid-block mechanism with finite element limit analysis ( $H/D=1$ ,  $\phi'=20^\circ$ ,  $\gamma D/c'=1$ ,  $S/D=2.0$ , smooth interface).

- (a) Plastic multiplier field
- (b) Velocity plot
- (c) Rigid-block mechanism

Fig. 6. Comparison of rigid-block mechanism with finite element limit analysis ( $H/D=3$ ,  $\phi'=10^\circ$ ,  $\gamma D/c'=1$ ,  $S/D=2.0$ , smooth interface).

- (a) Plastic multiplier field
- (b) Power dissipation
- (c) Rigid-block mechanism

Fig. 7. Comparison of rigid-block mechanism with finite element limit analysis ( $H/D=3$ ,  $\phi'=10^\circ$ ,  $\gamma D/c'=1$ ,  $S/D=3.5$ , smooth interface).

- (a) Plastic multiplier field
- (b) Power dissipation
- (c) Rigid-block mechanism

Fig. 8. Numerical results from finite element limit analysis ( $H/D=3$ ,  $\phi'=10^\circ$ ,  $\gamma D/c'=1$ ,  $S/D=7.0$ , smooth interface).

- (a) Plastic multiplier field
- (b) Velocity plot

Fig. 9. Stability bounds for dual circular tunnels at  $H/D=1$  ( $\phi'=5^\circ$ ,  $10^\circ$ ,  $15^\circ$ ,  $20^\circ$ , smooth interface).

- (a)  $\phi'=5^\circ$
- (b)  $\phi'=10^\circ$
- (c)  $\phi'=15^\circ$
- (d)  $\phi'=20^\circ$

Fig. 10. Stability bounds for dual circular tunnels at  $H/D=3$  ( $\phi'=5^\circ$ ,  $10^\circ$ ,  $15^\circ$ ,  $20^\circ$ , smooth interface).

- (a)  $\phi'=5^\circ$
- (b)  $\phi'=10^\circ$
- (c)  $\phi'=15^\circ$
- (d)  $\phi'=20^\circ$

Fig. 11. Stability bounds for dual circular tunnels at  $H/D=5$  ( $\phi'=5^\circ$ ,  $10^\circ$ ,  $15^\circ$ ,  $20^\circ$ , smooth interface).

- (a)  $\phi'=5^\circ$

- (b)  $\phi'=10^\circ$
- (c)  $\phi'=15^\circ$
- (d)  $\phi'=20^\circ$

Fig. 12. Relationship between critical tunnel spacing  $S/D$  and  $H/D$  ( $\phi'=5^\circ, 10^\circ, 15^\circ, 20^\circ$ , smooth interface).

- (a)  $\phi'=5^\circ$
- (b)  $\phi'=10^\circ$
- (c)  $\phi'=15^\circ$
- (d)  $\phi'=20^\circ$

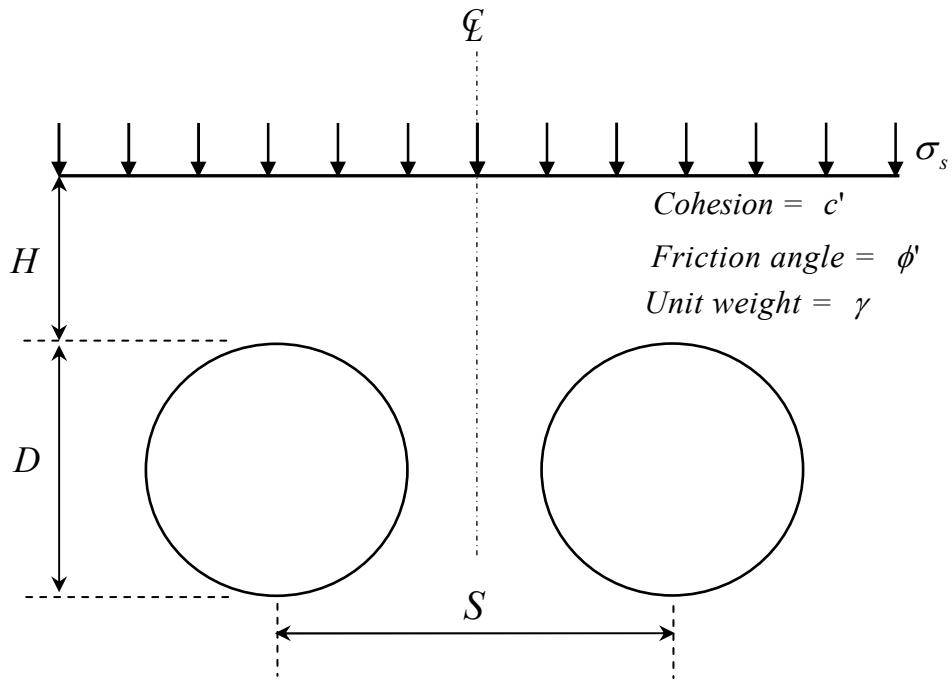


Fig. 1. Plane-strain dual circular tunnels in cohesive-frictional soil.

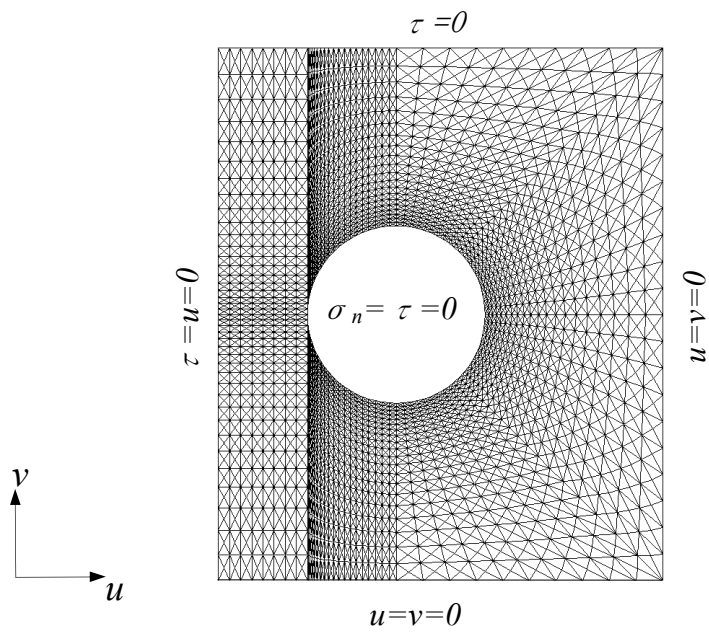
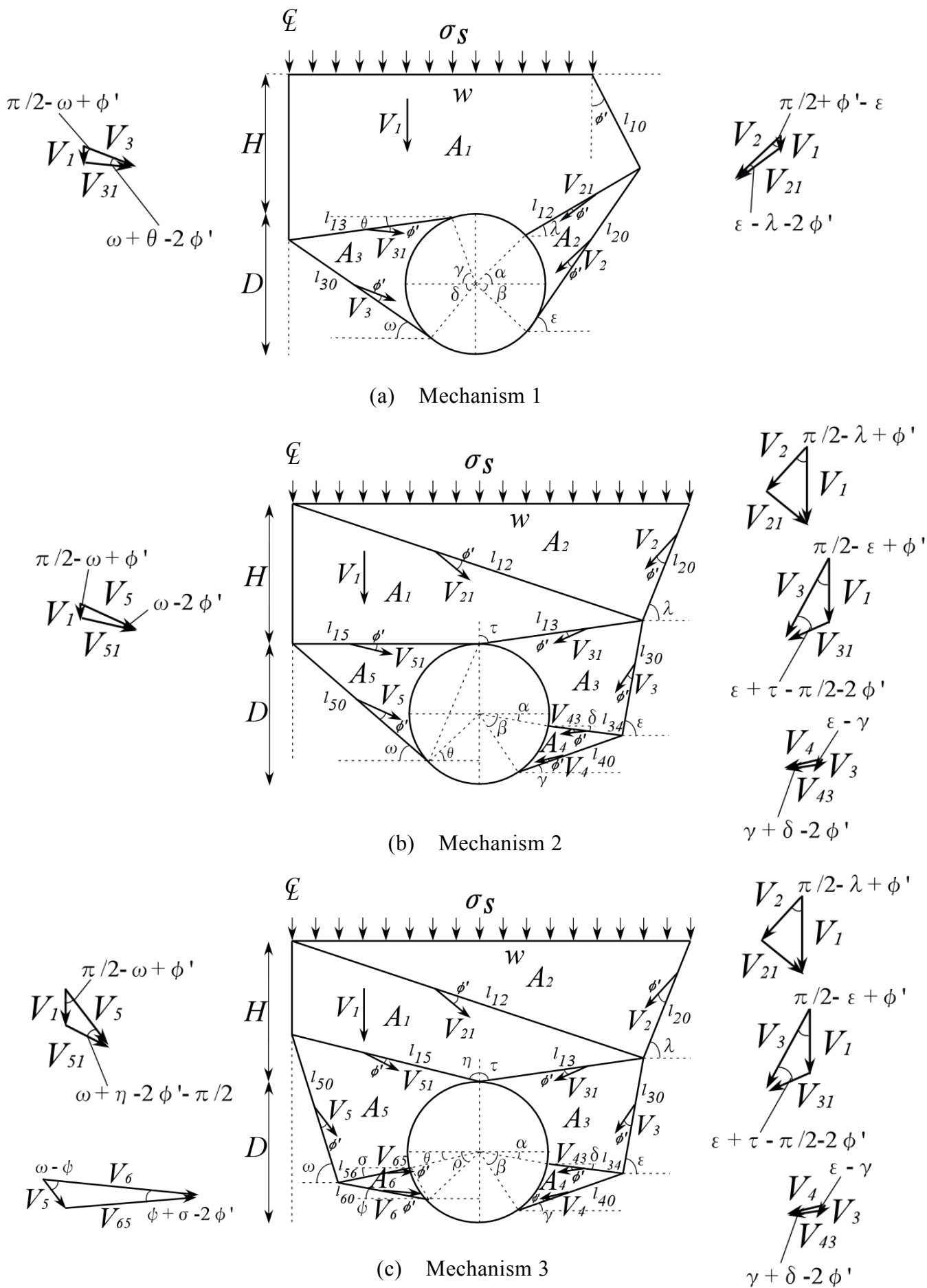
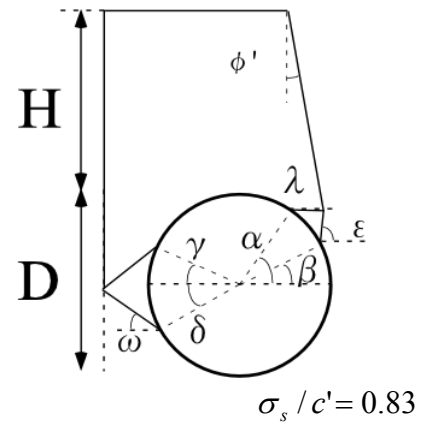
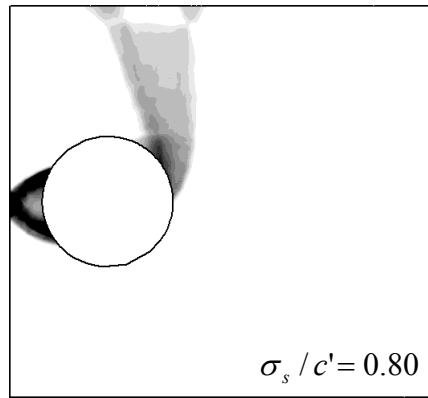
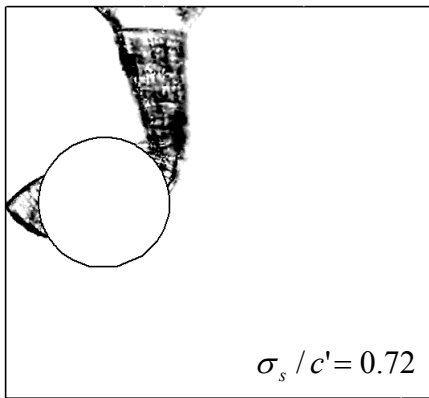


Fig. 2. Finite element mesh for  $H/D=1$  and  $S/D=2$  showing boundary conditions for numerical limit analysis.



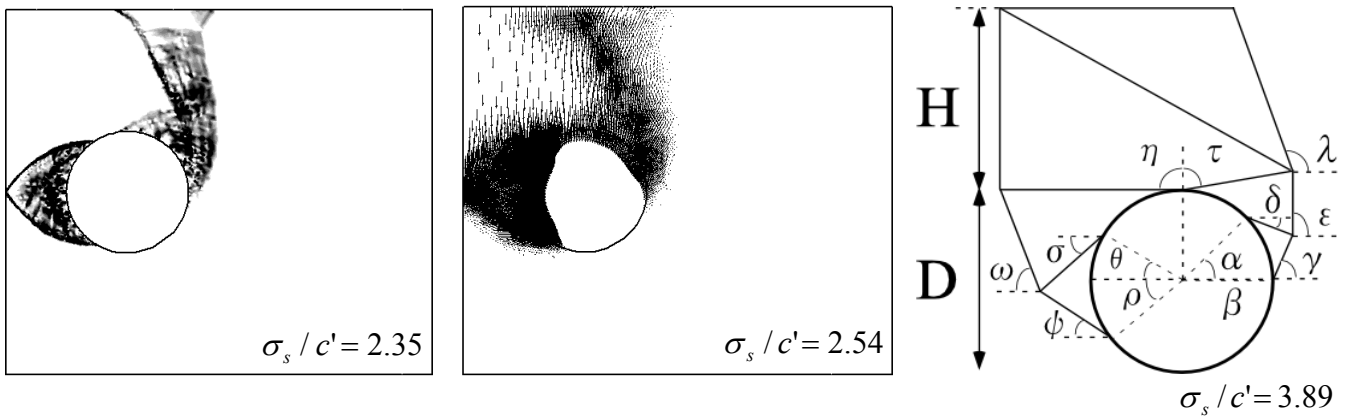


(a) Plastic multiplier field

(b) Power dissipation

(c) Rigid-block mechanism

Fig. 4. Comparison of rigid-block mechanism with finite element limit analysis  
 ( $H/D=1, \phi'=10^\circ, \gamma D/c'=1, S/D=1.5$ , smooth interface).

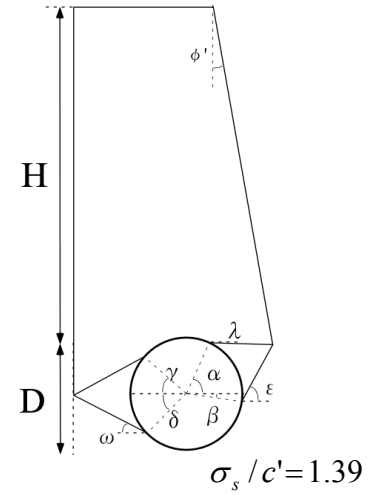
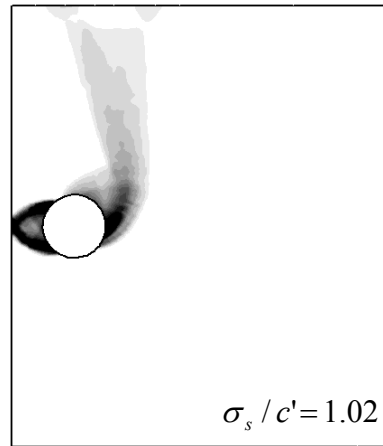
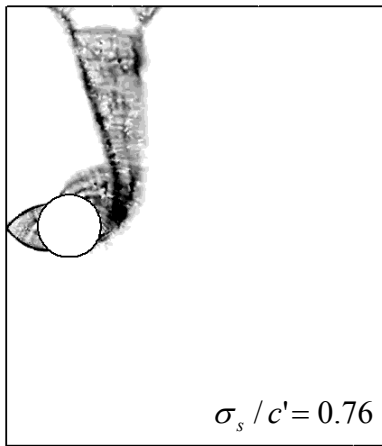


(a) Plastic multiplier field

(b) Velocity plot

(c) Rigid-block mechanism

Fig. 5. Comparison of rigid-block mechanism with finite element limit analysis  
 ( $H/D=1, \phi'=20^\circ, \gamma D/c'=1, S/D=2.0$ , smooth interface).



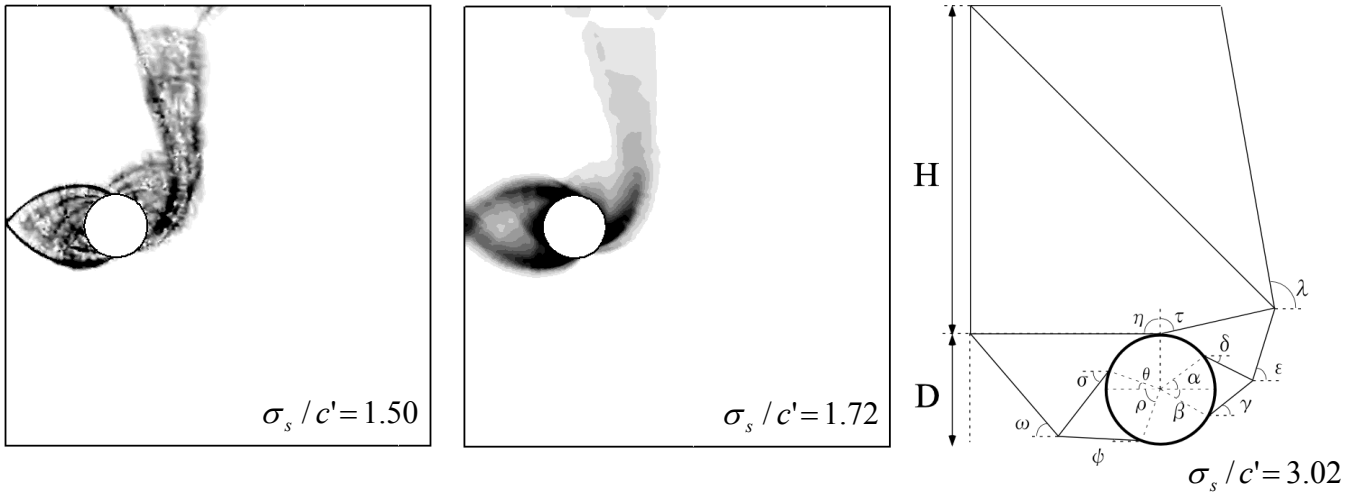
(a) Plastic multiplier field

(b) Power dissipation

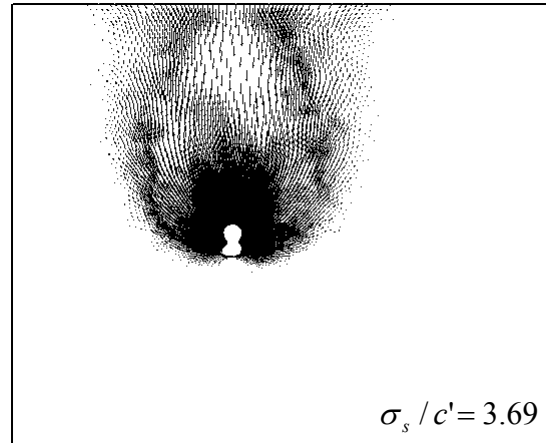
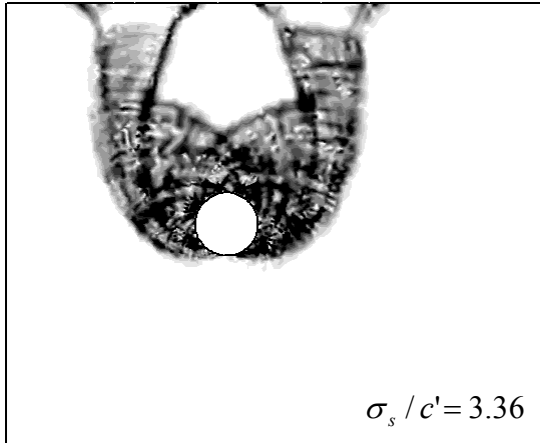
(c) Rigid-block mechanism

Fig. 6. Comparison of rigid-block mechanism with finite element limit analysis ( $H/D=3, \phi'=10^\circ, \gamma D/c'=1, S/D=2.0$ , smooth interface).





(a) Plastic multiplier field      (b) Power dissipation      (c) Rigid-block mechanism  
 Fig. 7. Comparison of rigid-block mechanism with finite element limit analysis  
 ( $H/D=3, \phi'=10^\circ, \gamma D/c'=1, S/D=3.5$ , smooth interface).



(a) Plastic multiplier field

(b) Velocity plot

Fig. 8. Numerical results from finite element limit analysis  
 ( $H/D=3, \phi'=10^\circ, \gamma D/c'=1, S/D=7.0$ , smooth interface).

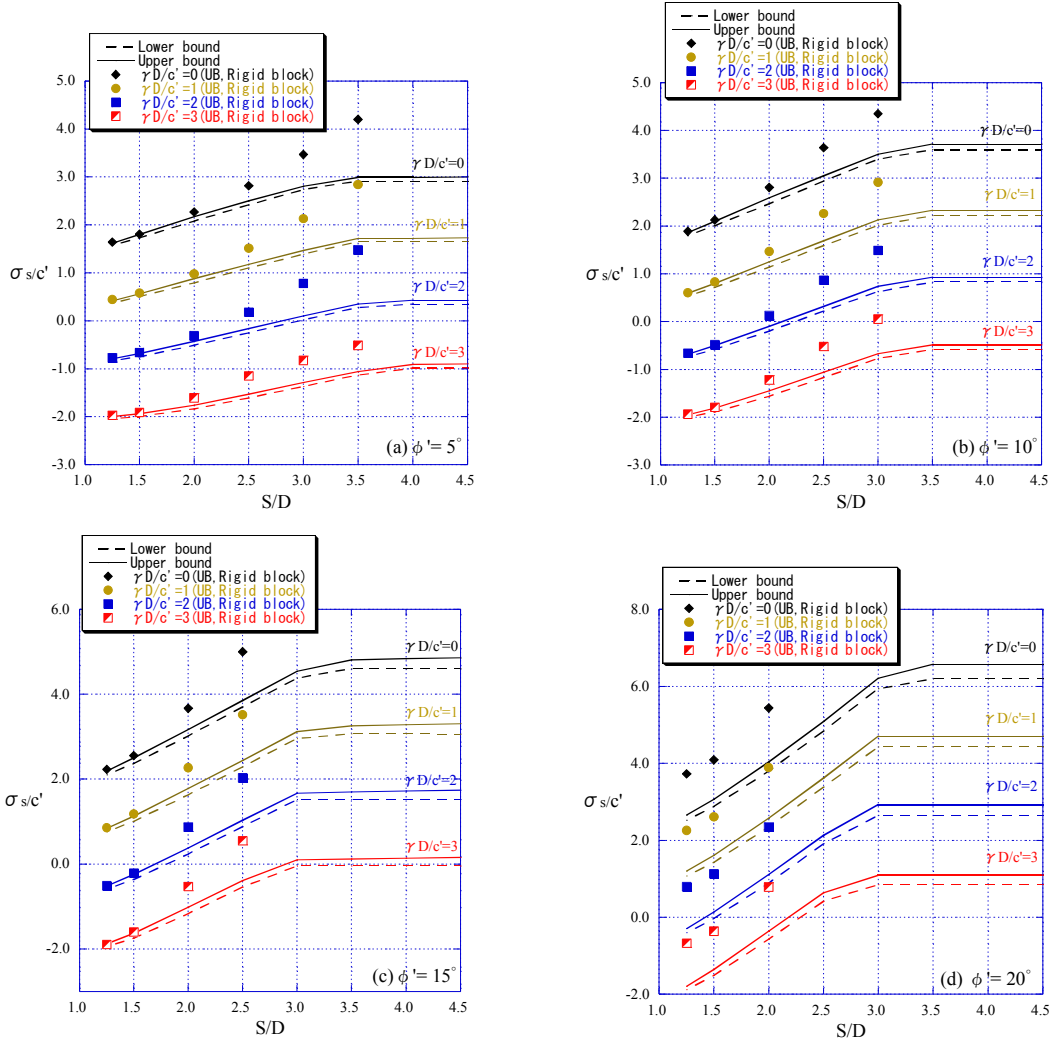


Fig. 9. Stability bounds for dual circular tunnels at  $H/D=1$  ( $\phi'=5^\circ, 10^\circ, 15^\circ, 20^\circ$ , smooth interface).

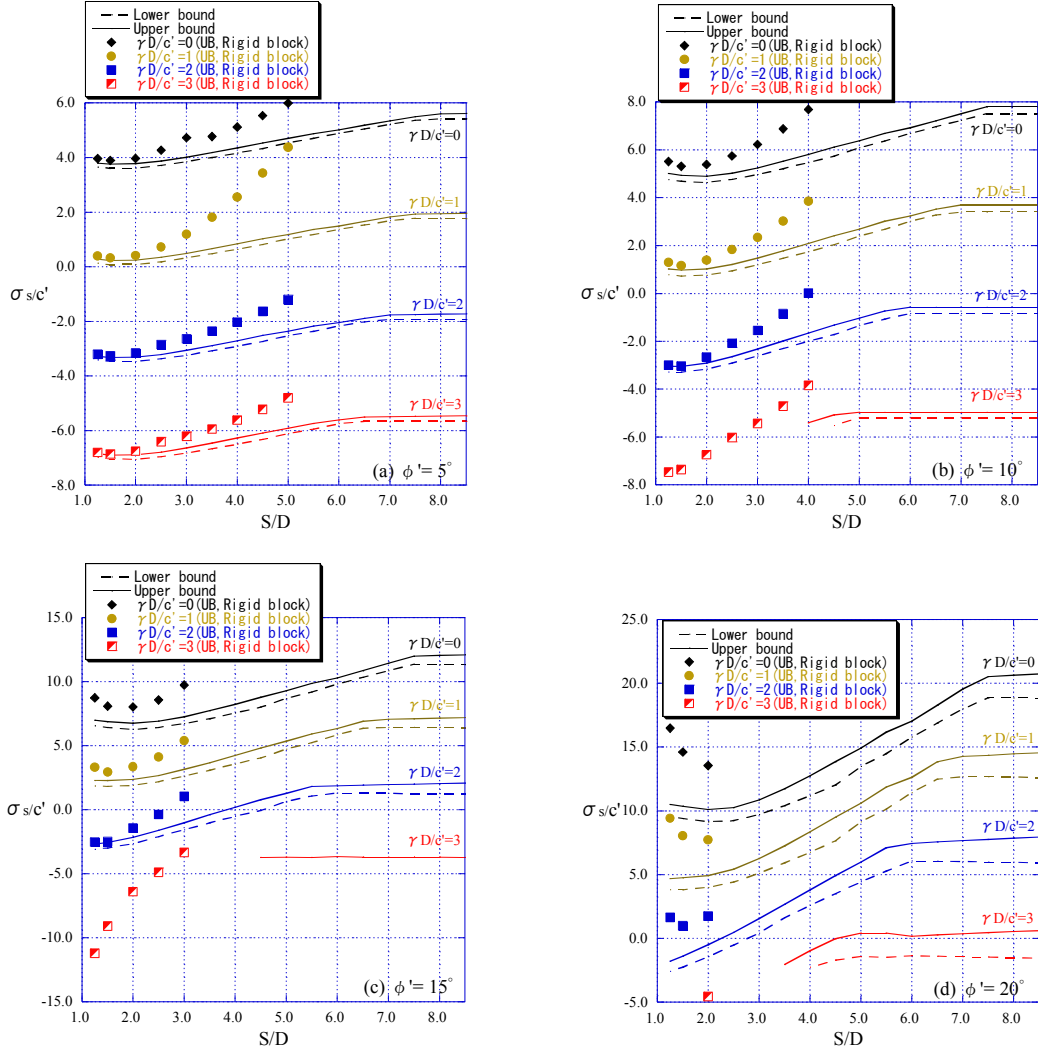


Fig. 10. Stability bounds for dual circular tunnels at  $H/D=3$  ( $\phi'=5^\circ, 10^\circ, 15^\circ, 20^\circ$ , smooth interface).

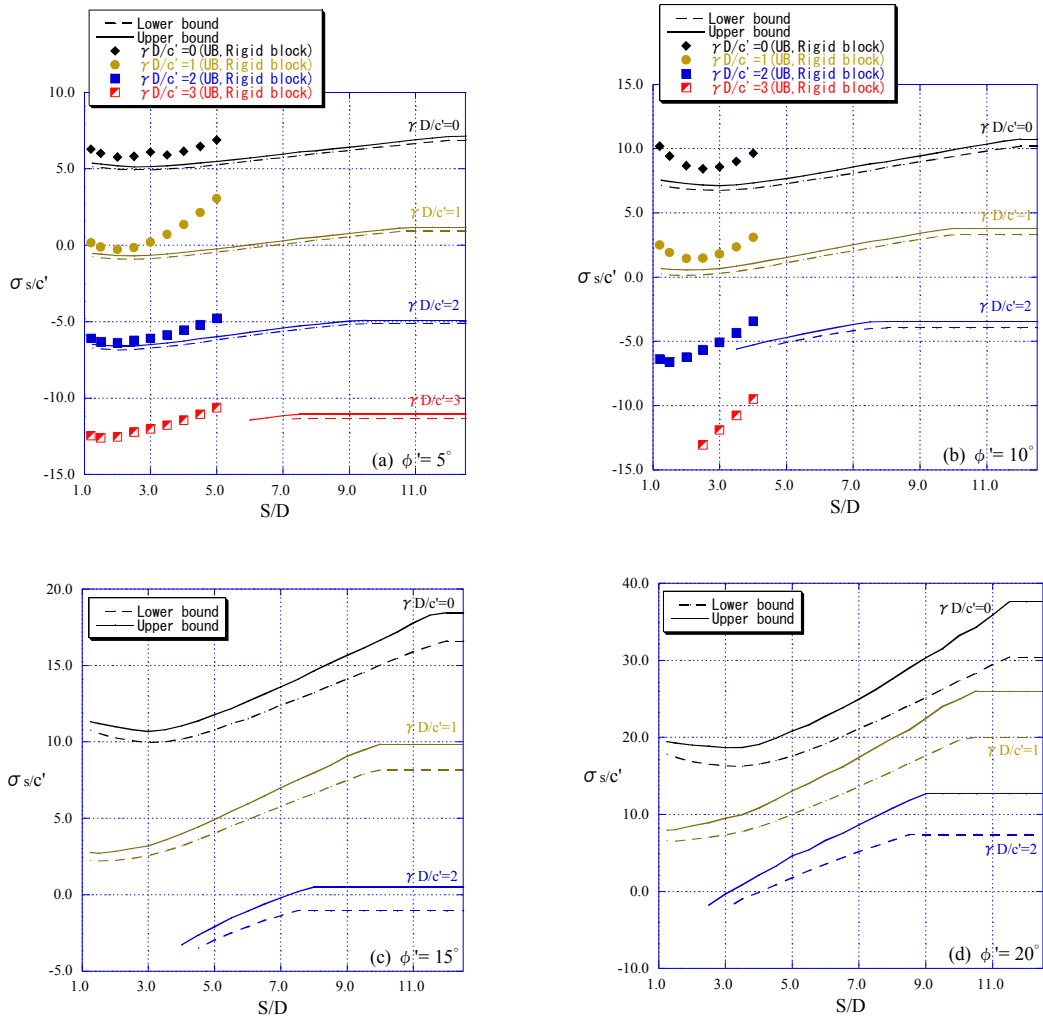


Fig. 11. Stability bounds for dual circular tunnels at  $H/D=5$  ( $\phi'=5^\circ, 10^\circ, 15^\circ, 20^\circ$ , smooth interface).

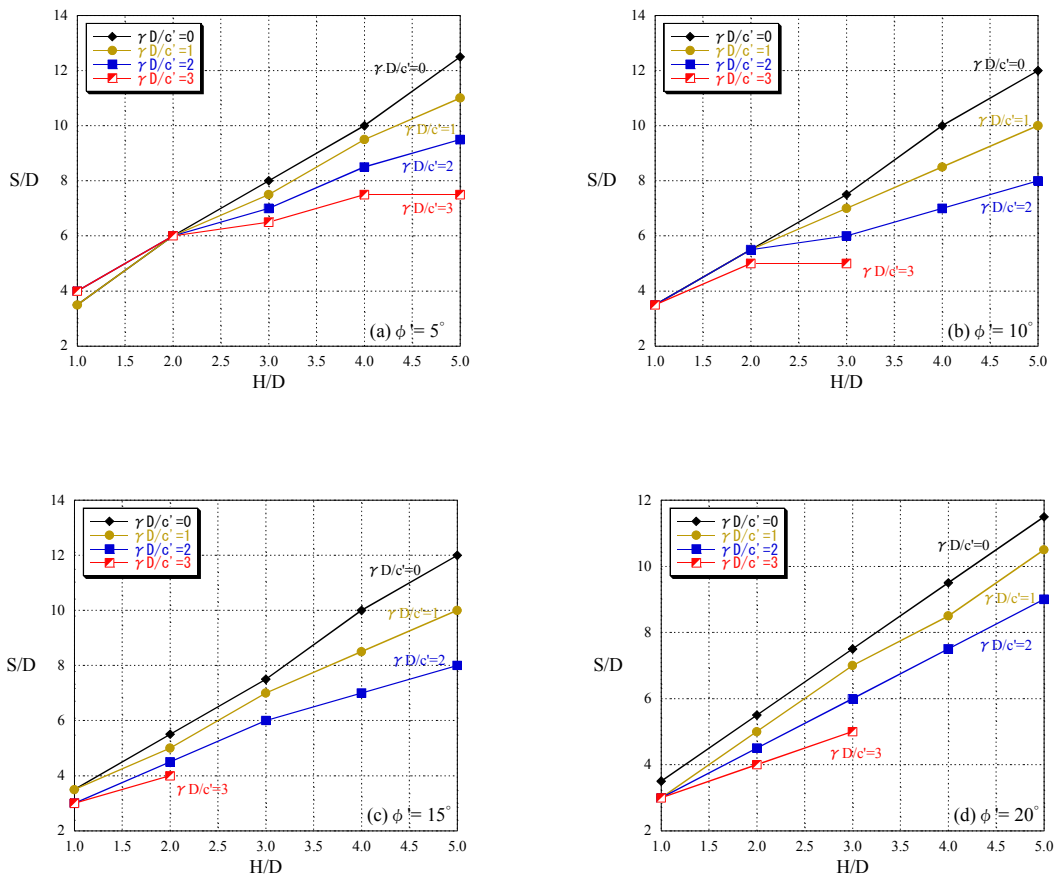


Fig. 12. Relationship between critical tunnel spacing  $S/D$  and  $H/D$  ( $\phi'=5^\circ, 10^\circ, 15^\circ, 20^\circ$ , smooth interface).